1-2006

Sequential Binding of Cobalt(II) to Metallo-β-lactamase CcrA

Gopal R. Periyannan
Miami University - Oxford

Alison L. Costello
University of New Mexico

David L. Tierney
University of New Mexico

Ke-Wu Yang
Miami University - Oxford

Brian Bennett
Marquette University, brian.bennett@marquette.edu

See next page for additional authors

Biochemistry, Vol. 45, No. 4 (1 January 2006): 1313–1320. DOI.

Sequential Binding of Cobalt(II) to Metallo-β-lactamase CcrA

Gopal R. Periyannan
Department of Chemistry and Biochemistry, Miami University, Oxford, Ohio
Alison L. Costello
Department of Chemistry, University of New Mexico, Albuquerque, New Mexico
David L. Tierney
Department of Chemistry, University of New Mexico, Albuquerque, New Mexico
Ke-Wu Yang
Department of Chemistry and Biochemistry, Miami University, Oxford, Ohio
Brian Bennett
National Biomedical EPR Center, Department of Biophysics, Medical College of Wisconsin, Milwaukee, Wisconsin
Michael W. Crowder
Department of Chemistry and Biochemistry, Miami University, Oxford, Ohio

SUBJECTS:
Peptides and proteins, Metals, Ions, Extended X-ray absorption fine structure

Abstract

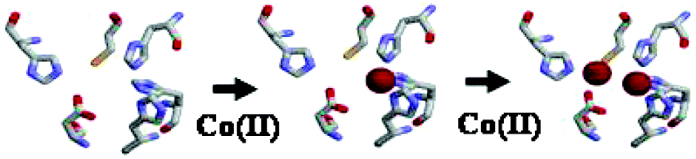

In an effort to probe Co(II) binding to metallo-β-lactamase CcrA, EPR, EXAFS, and ^{1}H NMR studies were conducted on CcrA containing 1 equiv (1-Co(II)-CcrA) and 2 equiv (Co(II)Co(II)-CcrA) of Co(II). The EPR spectra of 1-Co(II)-CcrA and Co(II)Co(II)-CcrA are distinct and indicate 5/6-coordinate Co(II) ions. The EPR spectra also reveal the absence of significant spin-exchange coupling between the Co(II) ions in Co(II)Co(II)-CcrA. EXAFS spectra of 1-Co(II)-CcrA suggest 5/6-coordinate Co(II) with two or more histidine ligands. EXAFS spectra of Co(II)Co(II)-CcrA also indicate 5/6 ligands at a similar average distance to 1-Co(II)-CcrA, including an average of about two histidines per Co(II). ^{1}H NMR spectra for 1-Co(II)-CcrA revealed seven paramagnetically shifted resonances, three of which were solvent-exchangeable, while the NMR spectra for Co(II)Co(II)-CcrA showed at least 16 shifted resonances, including an additional solvent-exchangeable resonance and a resonance at 208 ppm. The data indicate sequential binding of Co(II) to CcrA and that the first Co(II) binds to the consensus Zn_1 site in the enzyme.

Enzymes that hydrolyze β-lactam- containing antibiotics, such as penicillins, cephalosporins, and carbapenems, are called β-lactamases, and the production of β-lactamases by bacteria is the most common way that bacteria become antibiotic-resistant. Since β-lactam-containing compounds account for almost 50% of the available, effective antibiotics used in the clinic (*1*–*3*), bacterial resistance to these compounds is a serious public health issue. There are currently over 300 known β-lactamases, and several attempts have been made to classify these enzymes into four distinct groups based on molecular properties (*4*–*9*). Groups A, C, and D (or 1, 2, and 4) are similar in that these enzymes utilize an active site serine as a nucleophile in the hydrolysis reaction. The remaining group (B or 3) is often called metallo-β-lactamases (MβL's)[1] because the enzymes require 1−2 Zn(II) ions for full catalytic activity (*5*, *10*–*13*. MβL's constitute an ever-growing and troubling class of β-lactamases that have been found in clinical isolates of *Bacillus anthracis*, *Pseudomonas aeruginosa*, *Klebsiella pneumoniae*, and several other pathogens (*10*–*14*). MβL's contain 1−2 mol of Zn(II)/mol of enzyme, hydrolyze all known cephalosporins, carbapenems, and penicillins, are not inhibited by clavulanic acid and other classical β-lactamase inhibitors, and have no known clinically useful inhibitor toward them.

Previous studies have shown that there is significant structural and mechanistic diversity among the MβL's, leading to the grouping of the enzymes into three distinct subclasses (*15*) based on amino acid sequence identity at the Zn(II) binding sites. The B1 enzymes have a Zn_1 site consisting of His116, His118, and His196 and a Zn_2 site consisting of Asp120, Cys221, and His263 and are represented by metallo-β-lactamase CcrA from *Bacteroides fragilis* (*16*) (Figure 1), the B2 enzymes have the same metal binding sites as the B1 enzyme except that His116 is replaced by an Asn and are represented by metallo-β-lactamase ImiS from *Aeromonas sobria* (*17*), and the B3 enzymes have the same metal binding sites as the B1 enzymes except Cys221 is replaced with His121 and are represented by metallo-β-lactamase L1 from *Stenotrophomonas maltophilia* (*18*). The structural diversity among

the MβL's suggests that one inhibitor may not be effective in treating infections caused by bacteria that produce a metallo-β-lactamase. To address this question, we are currently characterizing a metallo-β-lactamase from each of the group B subgroups (CcrA, ImiS, and L1) in an effort to identify common structural/mechanistic properties of the enzymes toward which a single inhibitor can be designed.

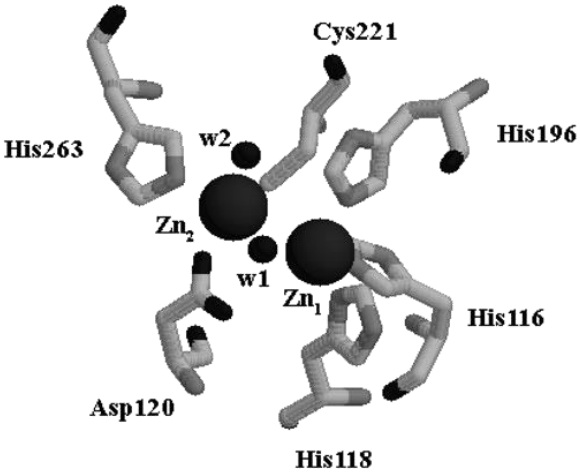

Figure 1 Active site structure of CcrA (*16*). The small sphere labeled W1 is a bridged hydroxide/water ligand, and W2 is a terminally bound water ligand. The figure was prepared using Rasmol version 2.7 (R. Sayle, 1994, Greenford, Middlesex, U.K.) and the crystal coordinates of CcrA (PDB code 1ZNB).

There is considerable information available on MβL's, such as X-ray crystal structures (*18*−*21*) and spectroscopic, mechanistic, (*22*−*30*), and computational studies (*31*−*38*). Nonetheless, there are long-standing questions about the MβL's dealing with substrate binding, reaction mechanism, and the number of metal ions in the physiologically relevant enzymes. We are currently using rapid freeze-quench spectroscopic studies to probe substrate binding and the mechanism of L1 and ImiS. Before these studies can be performed on CcrA, detailed spectroscopic characterization of the resting form of the enzyme is necessary. This work describes our efforts to characterize cobalt binding to CcrA by using spectroscopic methods.

Experimental Procedures

Materials

Escherichia coli strain BL21(DE3) was obtained from Novagen, Madison, WI. The overexpression plasmid for CcrA, pMSZ02, was generously supplied by Wang and Benkovic (*26*). Isopropyl β-d-thiogalactoside (IPTG) was purchased from Anatrace (Maumee, OH). A Minitan II concentrator system was purchased from Fisher Scientific, Pittsburgh, PA, and was equipped with four 10000 NMWL plates from Millipore, Bedford, MA. Protein solutions were concentrated with an Amicon ultrafiltration cell equipped with YM-10 DIAFLO membranes from Amicon, Inc., Beverly, MA. Dialysis tubing was prepared using Spectra/Por-regenerated cellulose molecular porous membranes with a molecular mass cutoff of 6000−8000 Da.

Metal-free buffers were prepared by treatment of buffers with Chelex 100 resin, purchased from Bio-Rad Laboratories, and filtration of the buffer through a 0.22 μm membrane from Osmonics, Inc. A fast protein liquid chromatography (FPLC) system and Q-Sepharose chromatography columns were purchased from Amersham Pharmacia Biotech. Nitrocefin was purchased from Becton Dickinson, and solutions of nitrocefin were filtered through a Fisherbrand 0.45 μm syringe filter. All buffers and media were prepared using Barnstead NANOpure ultrapure water.

Methods

Preparation of Co(II)-Substituted CcrA.

Soluble CcrA was overexpressed and purified according to Wang and Benkovic (*26*). Protein concentrations were determined by using $\varepsilon_{280\ nm}$ = 39000 M^{-1} cm^{-1} and Beer's law. Apo-CcrA was prepared by dialyzing purified CcrA (0.4−0.5 mM) versus 3 × 1 L of 50 mM Hepes, pH 7.6, containing 10 mM EDTA, at 4 °C (12 h for each dialysis step). The use of phenanthroline, in place of EDTA, resulted in precipitation of CcrA. The chelating agent was removed by dialysis versus 8 × 1 L of metal-free, 50 mM Hepes, pH 7.6, at 4 °C. Metal analyses of the resulting enzyme solutions were used to verify that the enzymes contain <0.05 equiv of Zn(II). Apo-CcrA can be stored indefinitely at −70 °C after flash freezing in liquid nitrogen.

To prepare 1-Co(II)-CcrA, stoichiometric amounts of Co(II) were added directly to apo-CcrA. The rapid addition of highly concentrated $CoCl_2$ stocks to highly concentrated (>1 mM) apo-CcrA samples resulted in immediate precipitation of the protein. To circumvent this problem, NMR and EPR samples were prepared by slowly adding aliquots of $CoCl_2$ to relatively dilute solutions of apo-CcrA (∼300 μM). After 30 min incubations on ice, the CcrA samples were concentrated using a Centricon-10. During the preparation of EXAFS samples, the CcrA samples contained 20% (v/v) glycerol, and the addition of Co(II) to concentrated samples of apo-CcrA with glycerol did not result in precipitated protein. The EXAFS samples exhibited the same steady-state kinetic constants as the NMR and EPR samples. Preparation of Co(II)-substituted CcrA was performed in a glovebox under a nitrogen atmosphere. To prepare a Co(II)Co(II) form of CcrA, a second equivalent of Co(II) was added to 1-Co(II)-CcrA, and the sample was incubated at least 30 min before analysis.

Metal Analysis and Steady-State Kinetics.

The metal content of protein solutions was determined using a Varian Liberty 150 inductively coupled plasma spectrometer with atomic emission spectroscopy detection (ICP-AES). The protein samples were diluted to 10 μM with 50 mM Hepes, pH 7.6. A calibration curve with four standards and a correlation coefficient of greater than 0.999 was generated using Zn and Co reference solutions from Fisher Scientific. The following emission wavelengths were chosen to ensure the lowest detection limits possible: Zn, 213.856 nm, and Co, 238.892 nm.

Enzyme activity was determined in MTEN buffer (50 mM Mes, 25 mM Tris, 25 mM ethanolamine, and 100 mM NaCl) at pH 7.0 and 25 °C using nitrocefin as substrate. The formation of the hydrolyzed nitrocefin was monitored at 485 nm, and absorbance data were converted into concentration data by using an extinction coefficient of ε_{485nm} = 17400 M^{-1} cm^{-1}.

EPR Spectroscopy.

EPR spectra were recorded using a Bruker E500 EleXsys spectrometer equipped with an Oxford Instruments ESR-900 helium flow cryostat and a Bruker DM 4116 ER cavity operating at 9.6330 ± 0.0005 GHz. Data were collected at 12 K with 2 mW microwave power and 10.6 G magnetic field modulation at 100 kHz; these conditions were determined to be nonsaturating. Spectra were simulated by using XSophe simulation software (Bruker Biospin) and the spin Hamiltonian $H = \beta \mathbf{g} HS + \mathbf{S} DS$, explicitly assuming $S = {}^3/_2$. EPR samples were made by pipetting 400 μL of ca. 400 μM Co(II)-substituted CcrA into a 4 mm o.d. quartz EPR tube. Samples were prepared under a nitrogen environment in a glovebox, and the samples were frozen by slow immersion in a liquid nitrogen bath.

EXAFS Spectroscopy.

CcrA samples (1−2 mM) for EXAFS were prepared with 20% (v/v) glycerol as glassing agent, preloaded in Lucite cuvettes with 6 μm polypropylene windows, and frozen in liquid nitrogen. X-ray absorption spectra for 1-Co(II) and Co(II)Co(II) analogues of CcrA were measured on two individually prepared samples. As both samples gave comparable results, the two data sets for each analogue were averaged, and the averaged data are presented in Figure 3 (15 scans per sample). XAS data were measured at the National Synchrotron Light Source (NSLS),

beamline X9B, using a Si(111) double crystal monochromator; data collection and reduction were performed according to published procedures (*39*), using E_0 = 7725 eV. The resulting EXAFS data were fitted (∼9 deg of freedom for single-scattering and 30 for multiple-scattering models; see Table 1) using the nonlinear least-squares algorithm contained in the program IFEFFIT, interfaced with "SixPack" (available free of charge from http://www-ssrl.slac.stanford.edu/∼swebb/index.htm). The scale factor, S_c, and ΔE_0 were calibrated by fitting data for compounds of known structure, holding all other parameters fixed. Models used for calibration were bis[tris(pyrazolylborate)]cobalt(II), $CoTp_2$, for Co−N scattering and (tetramesitylthiolate)cobalt(II), $Co(Smes)_4$, for Co−S interactions. Optimum scale factors and ΔE_0's were Co−N, S_c = 0.74, ΔE_0 = −11, and Co−S, S_c = 0.85, ΔE_0 = −11.

Fits were carried out for all reasonable coordination numbers, holding S_c and ΔE_0 constant, while varying R_{as}, and σ_{as}^2. Multiple-scattering fits were performed according to published procedures (*40*), utilizing the pyrazole outer shell scattering of $CoTp_2$ for calibration. Briefly, multiple-scattering contributions were approximated by fitting FEFF calculated paths, derived from the crystallographic coordinates of $CoTp_2$, to the experimental EXAFS of $CoTp_2$. The best fits resulted in four prominent multiple-scattering features (representing 140 total scattering paths), and paths of similar overall length were combined to match these four features. Consequently, the labels in Table 1, while reflecting the greatest contributor to a combined path, are nonphysical. These combined paths were used to fit protein data, fixing the number of imidazole ligands per cobalt ion at half-integral values while varying R_{as} and σ_{as}^2.

NMR Spectroscopy.

The samples for NMR studies were made by loading 1 mM Co(II)-substituted CcrA into a 5 mm Wilmad NMR tube under a nitrogen environment in a glovebox. The buffer was Hepes, pH 7.0, containing ∼10% D_2O. Samples in 90% D_2O were made by performing three or more dilution/concentration cycles in a Centricon-10. NMR spectra were collected on a Bruker Avance 500 spectrometer operating at 500.13 MHz, 298 K, magnetic field of 11.7 T, recycle delay (AQ) of 41 ms, and sweep width of 400 ppm. Chemical shifts were referenced by assigning the H_2O signal the value of 4.70 ppm. A modified presaturation pulse sequence (zgpr) was used to suppress the proton signals originating from solvent. The presaturation pulse was the shortest possible (500 ms) to avoid saturation of solvent-exchangeable proton signals.

UV−Vis Spectrophotometry.

Apo-CcrA (360 μM) in 50 mM Hepes, pH 7.6, was titrated with an aqueous solution of $CoCl_2$ (Strem Chemicals, 99.999% pure). After the solution was incubated on ice for 30 min, the absorbance spectra were obtained with the buffer as a reference. UV−vis difference spectra were obtained by subtracting the spectrum of apo-CcrA from those of the Co(II)-added samples.

Results

Preparation of Co(II)-Substituted CcrA.

Purified, as-isolated CcrA contained 1.7 equiv of Zn(II), which is consistent with metal analyses reported by Yanchak et al. (*25*) and Yang et al. (*41*). Steady-state kinetic studies on multiple preparations of CcrA demonstrated that the enzyme exhibits a k_{cat} value of 221 s^{-1} and a K_m of 6.2 μM when using nitrocefin as the substrate. These steady-state kinetic values are similar to those reported by others (*25*, *26*, *41*−*44*. The steady-state kinetic constants k_{cat} and K_m for CcrA with 1 equiv of Co(II) added (1-Co(II)-CcrA) were 98 s^{-1} and 12 μM, respectively, while CcrA with 2 equiv of Co(II) added (Co(II)Co(II)-CcrA) exhibited values of 110 s^{-1} and 5 μM, respectively. These values are in excellent agreement with those previously published by Wang and Benkovic (*26*).

EPR Spectroscopy.

The EPR spectrum of 1-Co(II)-CcrA was obtained at 12.4 K (Figure 2). This spectrum is essentially axial, with a resolved $g_{eff(z)}$, and was well-simulated by assuming $S = {}^3/_2$, $M_s = \pm{}^1/_2$, $g_{x,y} = 2.27$, $g_z = 2.22$, and $E/D = 0.035$ (Figure 2B). These simulation parameters are consistent with a 5- or 6-coordinate Co(II) center in 1-Co(II)-CcrA, which is slightly distorted from axial symmetry. The EPR signal for 1-Co(II)-CcrA integrated to 1.0 equiv of Co(II). The small derivative feature at 1630 G was due to a trace Fe(III) contaminant and integrated to ≤0.01 spin; this was included in the simulation as an $S = {}^5/_2$ component with extensive strains in D and E/D. The EPR spectrum of Co(II)Co(II)-CcrA is different than that of 1-Co(II)-CcrA (Figure 2C) and integrates to 2.0 equiv Co(II). It appears to be overlapping spectra of at least two distinct signals, one of which is the spectrum of 1-Co(II)-CcrA. Therefore, the spectrum of 1-Co(II)-CcrA was subtracted from the spectrum of Co(II)Co(II)-CcrA, and the resulting difference spectrum is shown in Figure 2E. The subtracted spectrum was simulated by assuming $M_s = \pm{}^1/_2$, $g_{x,y} = 2.22$, $g_z = 2.40$, and $E/D = 0.005$ (Figure 2F). Summation of the simulated spectrum of 1-Co(II)-CcrA (Figure 2B) and the simulated spectrum of the subtracted spectrum (Figure 2F) results in spectrum D (Figure 2), which is a good fit to the experimental spectrum of Co(II)Co(II)-CcrA (Figure 2C). The EPR signal due to Co(II) in the second metal binding site of Co(II)Co(II)-CcrA (Figure 2E) is also essentially axial, and the simulation parameters indicate 5- or 6-coordination geometry for the Co(II). The very broad nature of the spectral features and, particularly, the unresolved $g_{eff(z)}$ feature indicate a higher degree of conformational flexibility than for the first site, possibly due to the binding of one or more solvent molecules. The distinct signals from Co_1 and Co_2 can be deconvoluted from the spectrum of Co(II)Co(II)-CcrA, and there is no evidence for significant spin-exchange coupling between the Co(II) ions in Co(II)Co(II)-CcrA.

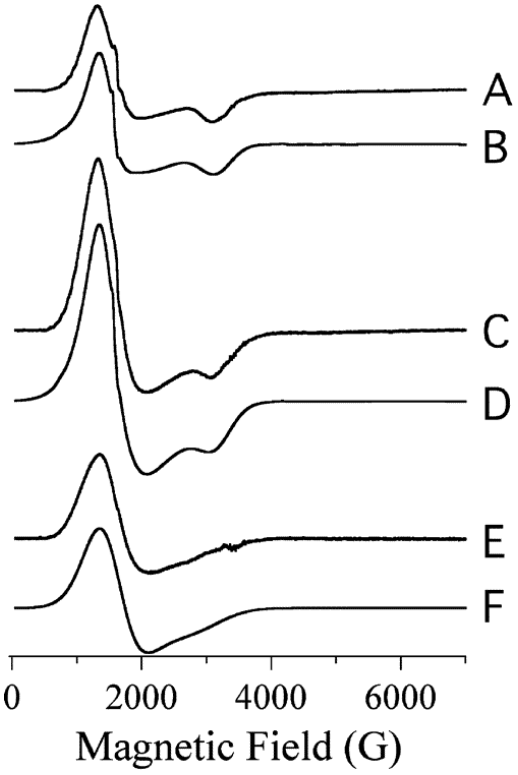

Figure 2 Experimental and simulated EPR spectra of Co(II)-substituted CcrA. Co(II)-substituted CcrA concentrations were 300 µM in 50 mM Hepes, pH 7.6. Experimental spectra are (A) 1-Co(II)-CcrA, (C) Co(II)Co(II)-CcrA, and (E) [2Co − 1Co]-CcrA, and spectra B, D, and F are computer simulations of spectra A, C, and E, respectively.

EXAFS Spectroscopy.

To further elucidate the structure of Co(II)-substituted CcrA, EXAFS data were collected for both 1-Co(II)- and Co(II)Co(II)-CcrA. Fourier transforms (FTs, solid lines in Figure 3, left) of k^3-weighted EXAFS data (solid lines in Figure 3, right) are presented overlaid with the best fits (dotted lines); curve fitting results are summarized in Table 1. The data for 1-Co(II)-CcrA (top half of Figure 3) were best fitted with a mixed first shell of two O (2.08 Å) and three N (2.20 Å) ligands to Co(II). The average first-shell bond length is too long to be consistent with a 4-coordinate cobalt ion. Inclusion of a sulfur ligand in the first shell leads to an increase in the fit residual, indicating sulfur is not bound to the first equivalent of cobalt bound by CcrA. Multiple-scattering fits indicate 2.0 ± 0.5 histidines bound to the Co(II) ion in 1-Co(II)-CcrA; the fit shown in the top half of Figure 3 corresponds to fit 3 in Table 1. A model that includes three similarly coordinated histidines gives a fit residual only 5% larger than the two His model presented. The ordered outer shell scattering indicates well-ordered binding of the first Co(II) ion to CcrA, and the data are most consistent with binding at the consensus Zn_1 site.

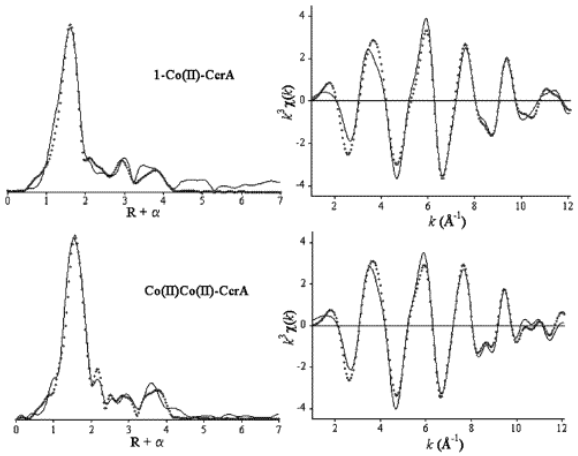

Figure 3 Fourier transforms (left) of experimental EXAFS spectra (right) for 1-Co(II)CcrA (top) and Co(II)Co(II)CcrA (bottom). Experimental data are presented as solid lines; fits are presented as open diamonds.

Table 1: EXAFS Curve Fitting Results for 1-Co-CcrA and Co(II)Co(II)-CcrA[a]

	model	Co−N	Co−O	Co−S	Co−His[b]	Co−C_{CO2-}	R_f[c]	R_u
	1-Co(II)-CcrA							
1	5 N/O	2.14 (5.1)					31	160
2	3 N + 2 O	2.20 (6.6)	2.08 (1.8)				19	155
3	3 N + 2 O + 2 His	2.19 (5.3)	2.08 (3.0)		2.92 (31), 3.39 (11), 4.13 (14), 4.36 (9)		62	93
	Co(II)Co(II)-CcrA							
4	5 N/O	2.14 (7.7)					33	136
5	3 N + 2 O	2.20 (4.1)	2.04 (1.4)				18	124
6	3 N + 2 O + 0.5 S	2.20 (0.5)	2.04 (0.1)	2.58 (19)			30	115
7	3 N + 2 O + 2.5 His	2.19 (2.0)	2.03 (0.9)		2.84 (15), 3.35 (18), 4.06 (12), 4.31 (10)		60	68
8	3 N + 2 O + 2.5 His + 1 C_{CO2-}	2.20 (2.0)	2.03 (0.6)		2.99 (10), 3.33 (15), 4.05 (11), 4.31 (10)	2.48 (0.6)	44	53

[a] Distances (Å) and disorder parameters [in parentheses, σ^2 (10^{-3} Å^2)] shown derive from integer or half-integer coordination number fits to filtered EXAFS data: k = [1, 12.1]; R = [0.9, 2.2] for single-scattering fits, and R = [0.1, 4.3] for multiple-scattering fits.[b] Multiple-scattering paths represent the combined paths described in Experimental Procedures. The labels indicate the individual path with largest amplitude, of those included in the combined path.[c] Goodness of fit (R_f for fits to filtered data and R_u for fits to unfiltered data) is defined as $1000\{[\mathrm{Re}(\chi_{i\mathrm{calc}})]^2 + [\mathrm{Im}(\chi_{i\mathrm{calc}})]^2\}/\{[\mathrm{Re}(\chi_{i\mathrm{obs}})]^2 + [\mathrm{Im}(\chi_{i\mathrm{obs}})]^2\}$, where N is the number of data points.

For Co(II)Co(II)-CcrA (Figure 3, bottom), the EXAFS data are best fitted with a 5-coordinate model that includes a mixed first shell of two O (2.04 Å) and three N (2.20 Å) ligands per metal ion, similar to the result for 1-Co(II)-CcrA. The outer shell scattering is significantly more ordered for Co(II)Co(II)-CcrA, consistent with the lower *E*/*D* shown above for the second Co(II) ion bound by CcrA. Fits, summarized in Table 1, indicate an average of 2.0 ± 0.5 histidines per Co(II) ion, similar to the number of coordinated histidines shown in the crystal structure of Zn(II)Zn(II)-CcrA (*16*). A new feature at $R + \alpha$ of 2.1 Å can also be seen for Co(II)Co(II)-CcrA, and this feature is adequately modeled with a single carbon atom at 2.48 Å, consistent with monodentate coordination of Asp120 by the second cobalt ion.

Although we expect the presence of, on average, 0.5 sulfur ligand per metal ion, inclusion of a sulfur scatterer, in either filtered first shell fits or multiple-scattering fits, does not significantly improve the fit residual (∼10%). Attempts to fit the feature ascribed to a carboxylate carbon, above, with 0.5 sulfur atom led to an unreasonable Co−S distance of >2.5 Å and an increase in the fit residual. Considering that the putative thiolate would comprise just 10% of the average coordination sphere of a cobalt ion in Co(II)Co(II)-CcrA, together with the heterogeneity indicated by first shell fits, and the overall complexity of the metal site, it may not be possible to detect the expected sulfur ligand. EXAFS studies of 5-coordinate mononuclear Co compounds with mixed (N_3OS) coordination suggest that this may be the case over the limited *k*-range typically available for metalloproteins (A. L. Costello and D. L. Tierney, unpublished results). A metal−metal scattering interaction at 3.60 Å could also be included in fits to the Co(II)Co(II)-CcrA EXAFS data; however, its inclusion is not statistically justified (∼12% improvement). While this may indicate that still higher quality data are required to determine the metal−metal distance in this system, it is also consistent with the lack of a covalent bridge connecting the two metal ions. Considering the lack of appreciable magnetic coupling between the cobalt ions, and the relatively high coordination number indicated both by the EPR and by the first shell fits, we favor the latter interpretation.

NMR Spectroscopy.

The ^{1}H NMR spectra of 1-Co(II)-CcrA and Co(II)Co(II)-CcrA are shown in panels A and B of Figure 4, respectively. Duplicate spectra were also obtained for samples in buffer containing ∼90% D_2O to identify any solvent-exchangeable protons. The spectrum of 1-Co(II)-CcrA has only seven hyperfine-shifted peaks (Figure 4). The chemical shifts of these peaks are consistent with these resonances originating from protons of metal-bound amino acid ligands. Among the seven peaks, three of them are solvent-exchangeable and can be assigned to three NH protons of metal-bound histidines. The appearance of three solvent-exchangeable peaks is consistent with the first Co(II) binding to the Zn_1 site, which has three histidine residues (Figure 4). Unambiguous assignment of the remaining four peaks in the NMR spectrum of 1-Co(II)-CcrA is difficult; however, they may be from four β-CH_2 protons of Co(II)-bound histidine residues. The most likely histidines are His116 and His196, which bind to Co(II) through Nε2 (*16*). The signals of ortho protons of Co(II)-bound histidines and the two β-CH_2 protons of His118 may be broadened beyond detection due to their close proximity to the paramagnetic center.

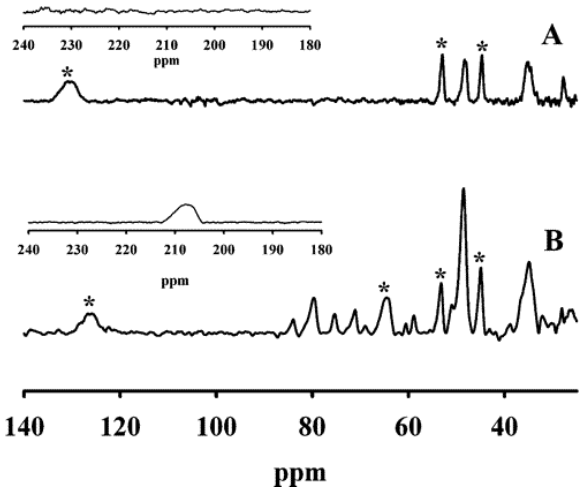

Figure 4 ^{1}H NMR spectra of Co(II)-substituted CcrA: (A) 1-Co(II)-CcrA and (B) Co(II)Co(II)-CcrA. The solvent-exchangeable proton signals are indicated by asterisks.

The NMR spectrum of Co(II)Co(II)-CcrA has 16 shifted peaks including the 7 peaks observed in the 1-Co(II)-CcrA spectrum (Figure 4). The most important features in this spectrum are the appearance of an additional solvent-exchangeable peak at 65 ppm and a broad peak at 208 ppm. The presence of these peaks clearly demonstrates that the second equivalent of Co(II) binds to a distinct site, and the additional solvent exchangeable resonance strongly suggests that the second Co(II) is bound to the Zn_2 site, which has only one histidine (Figure 1). Addition of the second equivalent of Co(II) also alters the chemical shift of one of the solvent-exchangeable protons identified for 1-Co(II)-CcrA (from 130 to 125 ppm), demonstrating a slight rearrangement of the metal site on binding the second metal ion. However, Co(II) binding to the Zn_2 site was expected to give rise to only six additional peaks (two β-CH_2 and an NH from His263 and two β-CH_2 and the α-CH of Asp120) instead of the additional nine peaks observed. A plausible explanation for this observation comes from the EXAFS and EPR data. The EXAFS studies suggest 5- or 6-coordination for both Co(II) ions, and EPR also indicates that the two Co(II) sites are either 5- or 6-coordinate. This larger coordination sphere, relative to native Zn(II) in Zn(II)Zn(II)-CcrA, would result in an increased distance between the ortho protons of metal-bound histidines and the cobalt ions in Co(II)Co(II)-CcrA and in the appearance of additional peaks.

UV−Vis Spectrophotometry.

The UV−vis difference spectra of CcrA containing 0.5, 1.0, and 2.0 equiv of Co(II) at pH 7.6 are shown in Figure 5. Identical spectra were obtained at pHs of 6.0 and 7.0 (data not shown). The addition of 0.5 equiv of Co(II) to apo-CcrA resulted in a broad signal between 450 and 650 nm, with an extinction coefficient of 65 M^{-1} cm^{-1}. There is no evidence for a S−Co(II) LMCT (expected peak position at 320−340 nm). The addition of 1.0 and 2.0 equiv of Co(II) to apo-CcrA resulted in increases in the broad feature between 450 and 650 nm, and the extinction coefficient of the feature increased from 90 M^{-1} cm^{-1} [CcrA with 1 equiv of Co(II)] to 114 M^{-1} cm^{-1} [CcrA with 2 equiv of Co(II)]. In the spectrum of CcrA containing 2.0 equiv of Co(II), there does appear to be a small feature at 330 nm (see arrow in Figure 5); however, the low signal-to-noise ratio in the spectrum prevents an unequivocal assertion that this signal is due to a S to Co(II) LMCT. The addition of 3.0 equiv or more of Co(II) to apo-CcrA resulted in rapid formation of a precipitate. In addition, spectrophotometric titrations of concentrated samples of apo-CcrA (>500 μM) resulted in rapid precipitation of the enzyme.

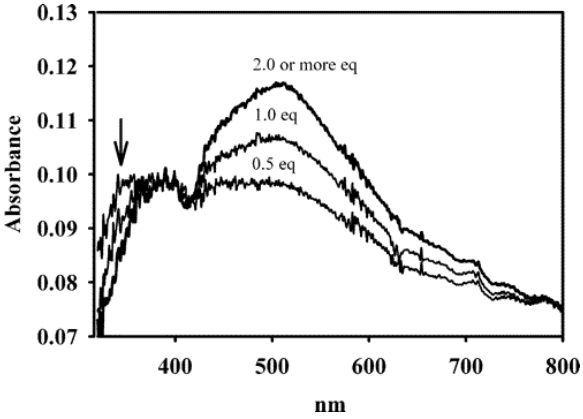

Figure 5 Spectrophotometric titration of apo-CcrA with Co(II). Apo-CcrA (360 μM) in 50 mM Hepes, pH 7.6, was titrated with 0.5, 1.0, and 2.0 equiv of Co(II). The spectrum of apo-CcrA was subtracted from the spectra of the Co(II)-added enzymes.

Discussion

Even though the crystal structures of most MβL's show proteins with dinuclear Zn(II) metal binding sites, there are many questions that remain about metal binding to these biomedically important enzymes. For example, several studies on metallo-β-lactamase BcII from *Bacillus cereus* indicated that the enzyme contained a high-affinity and a low-affinity metal binding site (*19*, *24*, *45*−*48*), suggesting that metal binding to this MβL would be sequential. This result was questioned by deSeny et al., who showed that the addition of Co(II) to the apoenzyme resulted in equal scrambling of the metal ions between the two metal binding sites (*49*). Wommer et al. furthered this study to suggest that physiologically relevant metal binding to several MβL's is probably substrate-dependent and that all MβL's are mononuclear Zn(II)-containing proteins in vivo (*50*). However, this hypothesis has recently been challenged by in vivo metal binding/protein expression studies (*51*). It is thus clear that many questions remain about metal binding to MβL's.

Previous spectrophotometric titrations of CcrA identified an absorption band that was assigned to a S → Co(II) ligand-to-metal charge transfer (LMCT) band that increased in intensity as Co(II) was added, from 0.5 to 2.0 equiv (*26*). Interestingly, activity versus metal content plots showed that CcrA is 83% as active as the fully loaded enzyme [Co(II)Co(II)-CcrA] with only 1 equiv of Co(II) added. There are a number of scenarios that can explain these apparently contradictory results. One possibility is that Co(II) distributes between the Zn_1 and Zn_2 binding sites as the apoenzyme is titrated with Co(II), resulting in Co(II) [Co(II) in the Zn_1 site] and Co(II) [Co(II) in the Zn_2 site] forms of the enzyme, which is the scenario that was predicted for BcII by deSeny et al. (*49*). This result would also suggest that either both mononuclear forms of CcrA are nearly fully active or that one form is fully active and the other is half as active as the fully loaded enzyme. Another possibility that could explain the previous spectrophotometric titrations and kinetics is that the first metal ion binds to a site that contains metal ligands from both metal binding sites. When the second metal ion binds, there would have to be a rearrangement of the metal binding site to accommodate the second metal ion. This form of the enzyme would have to be very active to account for the activity versus metal content data. One possibility that does not account for the previous data on CcrA is one with positive cooperativity in metal binding. In this case, CcrA samples containing 1 equiv of metal ion would consist of one-half fully loaded enzyme and one-half apoenzyme. Clearly, this possibility cannot adequately explain the activity versus metal content plots. In an effort to probe metal binding to CcrA, spectroscopic studies were used.

The EPR, EXAFS, and ^{1}H NMR studies reported here clearly indicate sequential, site-specific binding of Co(II) to our apo-CcrA. The EPR spectrum of 1-Co(II)-CcrA suggests 5/6-coordinate Co(II) in the first metal binding site.

The addition of a second Co(II) results in a distinct EPR signal, also indicative of 5/6-coordinate Co(II), but with higher conformational flexibility. Further, the signal due to Co_1 in 1-Co(II)-CcrA is identical in both form and intensity to the signal due to Co_1 in the spectrum of Co(II)Co(II)-CcrA. These data argue strongly that Co(II) binding to apo-CcrA is sequential. The signals from Co_1 and Co_2 exhibit no resolvable $I = {}^{7}/_{2}{}^{59}Co$ hyperfine splittings, consistent with the conformational flexibility anticipated for a site rich in unconstrained ligands, such as water. In the case of Co_1, such a ligand is required, as the activity data of Wang and Benkovic indicate that this is the hydrolytic metal ion (*26*). The even greater strain-dependent line widths in the signal from Co_2 are surprising considering the crystal structure of Zn(II)Zn(II)-CcrA (*16*), as they suggest an even less constrained ligand sphere, perhaps with a higher number of solvent-derived ligands. These EPR studies do not support the existence of any spin coupling between the Co(II)'s; however, spin coupling between two metal ions with only one bridging ligand would be expected to be very weak and not detectable with EPR studies.

The EXAFS suggest 5- or 6-coordination for the first-bound Co(II) ion, consistent with the EPR and UV−vis data and earlier electronic absorption in the d−d region (*26*). Multiple-scattering analyses indicate multiple histidine ligands, suggesting that the first Co(II) binds to the Zn_1 site in CcrA. The changes in shape of the outer shell scattering features for Co(II)Co(II)-CcrA, particularly the appearance of the feature assigned to a 2.5 Å Zn−C interaction from coordinated aspartate, clearly indicate that the average environment of the cobalt ions is different from that in 1-Co(II)-CcrA. This observation is inconsistent with nonsequential metal binding, which would be expected to give the same average structure for both the one- and two-metal forms of the enzyme. The data for Co(II)Co(II)-CcrA could not unequivocally define a M−M interaction, which we suggest indicates the absence of a bridging ligand in the di-Co enzyme. This result is consistent with the power and temperature dependence of the EPR, which showed no exchange coupling between the Co ions in Co(II)Co(II)-CcrA. Since the crystal structure of CcrA showed a bridging hydroxide and a 4-coordinate Zn_1 site and a 5-coordinate Zn_2 site (*16*), these data clearly indicate that Co(II) does not bind identically as Zn(II) in CcrA. The differing metal ion environments of the Co(II) versus the Zn(II) enzymes offer an explanation for the lower catalytic activity of the Co(II)-substituted enzyme, which is a common characteristic of most Co(II)-substituted, Zn(II) metalloenzymes (*39, 52*).

Examination of the ^{1}H NMR spectra of one Co-containing and two Co-containing CcrA provides the most compelling evidence for sequential metal binding to the enzyme. The NMR spectrum of 1-Co(II)-CcrA showed three solvent-exchangeable proton peaks, assigned to NH protons on Co(II)-bound histidines. The Zn_1 site in CcrA has three metal binding histidines (His116, His118, and His196) (*16*); therefore, the NMR studies strongly suggest that the first Co(II) binds in the Zn_1 site of the enzyme. The NMR spectrum of Co(II)Co(II)-CcrA exhibits the same three solvent-exchangeable proton resonances, along with one additional, solvent-exchangeable peak. Since the Zn_2 site in CcrA has one metal binding histidine residue (His263) (*16*), this result supports our conclusion that the second Co(II) binds to the Zn_2 site. The NMR spectrum of Co(II)Co(II)-CcrA also demonstrates an interesting new peak at 208 ppm. We cannot unambiguously assign this resonance at this point, although previous studies have suggested that β-CH_2 protons on Co(II)-bound cysteines can be found at resonance positions greater than 150 ppm (*53*). Nonetheless, the presence of the same nine hyperfine-shifted resonances in the spectra of 1-Co(II)CcrA and Co(II)Co(II)CcrA, with seven additional peaks in the spectrum for Co(II)Co(II)CcrA, provides the strongest evidence for well-ordered and sequential binding of metal ions by CcrA.

One particularly interesting result of these studies is the lack of direct evidence for a cysteine ligand bound to Co(II) in the EXAFS and UV−vis studies. Recently, crystal structures of BcII demonstrated that Cys221 can be oxidized to a *S*-cysteinesulfinic acid or *S*-hydroxycysteine (*54*). This same Cys was shown to be oxidized in the crystal structure of VIM-2 (PDB code 1KO2). The presence of significant amounts of oxidized Cys221 in CcrA could explain why a S to Co(II) LMCT was not observed in the UV−vis titrations or a S−Co(II) interaction was not observed in the EXAFS studies on Co(II)Co(II)-CcrA. However, unlike in BcII and VIM-2 where oxidized Cys221 is

probably not a metal binding ligand, CcrA with oxidized Cys221 can bind 2 equiv of metal, suggesting that this amino acid can potentially coordinate the second Co(II). The observed coordination numbers of Co(II) in 1-Co(II)-CcrA and in Co(II)Co(II)-CcrA suggest a high degree of flexibility in the metal binding sites of CcrA and may aid in reducing steric effects that prevent a second equivalent of metal from binding to BcII and VIM-2 with oxidized Cys221 residues. This flexibility in the metal binding site of CcrA may allow for coordination of the sulfur of oxidized Cys221 and lead to the assignment of the 208 ppm resonance in the NMR spectrum to β-CH_2 protons on Co(II)-bound, oxidized Cys221, although, to our knowledge, this scenario would be unprecedented in the literature. This flexibility in the Zn_2 metal binding site could lead to Co(II) binding to the sulfur atom of oxidized Cys221 in most molecules of CcrA and to the oxygen in others. The resulting mixture of proteins could explain why some of the NMR signals observed for Co(II)Co(II)-CcrA appear to integrate to less than one proton and why there are more signals than predicted by the crystal structure (*16*). As we strictly followed the purification protocol of CcrA as described by Wang et al. (*26*), it is not clear why our samples may contain oxidized cysteines and those previously reported do not. Our preparation of CcrA results in an enzyme that exhibits the same kinetic properties as previously reported and allows for sequential binding of Co(II), as clearly indicated by our EPR, EXAFS, and NMR data. The ability to sequentially bind Co(II) to CcrA now allows for the preparation and characterization of mixed metal analogues of CcrA (Co−CcrA, CoZn−CcrA, ZnCo−CcrA, and CoCo−CcrA) and allows for the elucidation of the roles of each metal ion in catalysis and substrate binding.

Acknowledgment

The authors thank Krishan Damodaran for collecting some additional NMR spectra and Tara K. Sigdel and J. Allen Easton for running some MALDI-TOF mass spectra.

References

1 Bush, K., and Mobashery, S. (1998) in *Resolving the Antibiotic Paradox* (Mobashery, R. A., Ed.) pp 71−98, Kluwer Academic/Plenum Publishers, New York.
2 Levy, S. B. (1998) The Challenge of Antibiotic Resistance, *Sci. Am.3*, 47−53.
3 Neu, H. C. (1992) The Crisis in Antibiotic Resistance, *Science257*, 1064−1073.
4 Ambler, R. P. (1980) The Structure of β-Lactamases, *Philos. Trans. R. Soc. London, Ser. B289*, 321−331.
5 Bush, K. (1998) Metallo-β-Lactamases: A Class Apart, *Clin. Infect. Dis. 27* (Suppl. 1), S48−S53.
6 Bush, K. (1989) Classification of β-Lactmases: Groups 1, 2a, 2b, and 2b', *Antimicrob. Agents Chemother.33*, 264−270.
7 Bush, K. (1989) Classification of β-Lactmases: Groups 2c, 2d, 2e, 3 and 4, *Antimicrob. Agents Chemother.33*, 271−276.
8 Bush, K., Jacoby, G. A., and Medeiros, A. A. (1995) A Functional Classification Scheme for β-Lactmases and Its Correlation with Molecular Structure, *Antimicrob. Agents Chemother. 39*, 1211−1233.
9 Rasmussen, B. A., and Bush, K. (1997) Carbapenem-Hydrolyzing β-Lactamases, *Antimicrob. Agents Chemother.41*, 223−232.
10 Cricco, J. A., Orellano, E. G., Rasia, R. M., Ceccarelli, E. A., and Vila, A. J. (1999) Metallo-β-lactamases: Does It Take Two to Tango?, *Coord. Chem. Rev.190−192*, 519−535.
11 Crowder, M. W., and Walsh, T. R. (1999) Metallo-β-lactamases: Structure and Function, *Res. Signpost3*, 105−132.
12 Payne, D. J. (1993) Metallo-β-lactamasesA New Therapeutic Challenge, *J. Med. Microbiol.39*, 93−99.
13 Wang, Z., Fast, W., Valentine, A. M., and Benkovic, S. J. (1999) Metallo-β-lactamases: Structure and Mechanism, *Curr. Opin. Chem. Biol.3*, 614−622.
14 Heinz, U., and Adolph, H. W. (2004) Metallo-β-lactamases: two binding sites for one catalytic metal ion?, *CMLS, Cell. Mol. Life Sci.61*, 2827−2839.
15 Galleni, M., Lamotte-Brasseur, J., Rossolini, G. M., Spencer, J., Dideberg, O., and Frere, J. M. (2001) Standard Numbering Scheme for Class B β-Lactamases, *Antimicrob. Agents Chemother.45*, 660−663.

16 Concha, N. O., Rasmussen, B. A., Bush, K., and Herzberg, O. (1996) Crystal Structure of the Wide-Spectrum Binuclear Zinc β-Lactamase from *Bacteroides fragilis*, *Structure4*, 823−836.
17 Walsh, T. R., Neville, W. A., Haran, M. H., Tolson, D., Payne, D. J., Bateson, J. H., MacGowan, A. P., and Bennett, P. M. (1998) Nucleotide and Amino Acid Sequences of the Metallo-*β*-lactamase, ImiS, from *Aeromonasveronii* bv. sobria, *Antimicrob. Agents Chemother.42*, 436−439.
18 Ullah, J. H., Walsh, T. R., Taylor, I. A., Emery, D. C., Verma, C. S., Gamblin, S. J., and Spencer, J. (1998) The Crystal Structure of the L1 Metallo-β-lactamase from *Stenotrophomonas maltophilia* at 1.7 Angstrom resolution, *J. Mol. Biol.284*, 125−136.
19 Carfi, A., Pares, S., Duee, E., Galleni, M., Duez, C., Frere, J. M., and Dideberg, O. (1995) The 3-D Structure of a Zinc Metallo-β-lactamase from *Bacillus cereus* Reveals a New Type of Protein Fold, *EMBO J.14*, 4914−4921.
20 Fitzgerald, P. M. D., Wu, J. K., and Toney, J. H. (1998) Unanticipated Inhibition of the Metallo-*β*-lactamase from *Bacteroides fragilis* by 4-Morpholineethanesulfonic Acid (MES): A Crystallographic Study at 1.85 Å Resolution, *Biochemistry37*, 6791−6800.
21 Fabiane, S. M., Sohi, M. K., Wan, T., Payne, D. J., Bateson, J. H., Mitchell, T., and Sutton, B. J. (1998) Crystal Structure of the Zinc-Dependent β-Lactamase from *Bacillus cereus* at 1.9 Å Resolution: Binuclear Active Site with Features of a Mononuclear Enzyme, *Biochemistry37*, 12404−12411.
22 Crowder, M. W., Wang, Z., Franklin, S. L., Zovinka, E. P., and Benkovic, S. J. (1996) Characterization of the Metal Binding Sites of the β-Lactamase from *Bacteroides fragilis*, *Biochemistry35*, 12126−12132.
23 Crowder, M. W., Yang, K. W., Carenbauer, A. L., Periyannan, G., Seifert, M. A., Rude, N. E., and Walsh, T. R. (2001) The Problem of a Solvent Exposable Disulfide When Preparing Co(II)-Substituted Metallo-*β*-lactamase L1 from *Stenotrophomonas maltophilia*, *J. Biol. Inorg. Chem.6*, 91−99.
24 Orellano, E. G., Girardini, J. E., Cricco, J. A., Ceccarelli, E. A., and Vila, A. J. (1998) Spectroscopic characterization of a binuclear metal site in *Bacillus cereus* β-lactamase II, *Biochemistry37*, 10173−10180.
25 Yanchak, M. P., Taylor, R. A., and Crowder, M. W. (2000) Mutational Analysis of Metallo-β-lactamase CcrA from *Bacteroides fragilis*, *Biochemistry39*, 11330−11339.
26 Wang, Z., and Benkovic, S. J. (1998) Purification, Characterization, and Kinetic Studies of Soluble Bacteroides fragilis Metallo-β-lactamase, *J. Biol. Chem.273*, 22402−22408.
27 Rasia, R. M., and Vila, A. J. (2003) Mechanistic Study of the Hydrolysis of Nitrocefin Mediated by *B. cereus* Metallo-β-lactamase, *ARKIVOC3*, 507−516.
28 McMannus-Munoz, S., and Crowder, M. W. (1999) Kinetic Mechanism of Metallo-β-lactamase L1 from *Stenotrophomonas maltophilia*, *Biochemistry38*, 1547−1553.
29 Garrity, J. D., Carenbauer, A. L., Herron, L. R., and Crowder, M. W. (2004) Metal Binding Asp-120 in Metallo-β-lactamase L1 from *Stenotrophomonas maltophilia* Plays a Crucial Role in Catalysis, *J. Biol. Chem.279*, 920−927.
30 Bounaga, S., Laws, A. P., Galleni, M., and Page, M. I. (1998) The Mechanism of Catalysis and the Inhibition of the *Bacillus cereus* Zinc-Dependent β-Lactamase, *Biochem. J.331*, 703−711.
31 Dal Peraro, M., Vila, A. J., and Carloni, P. (2003) Protonation State of Asp120 in the Binuclear Active Site of the Metallo-β-lactamase from *Bacteroides fragilis*, *Inorg. Chem.42*, 4245−4247.
32 Diaz, N., Suarez, D., and Merz, K. M. (2000) Zinc Metallo-β-lactamase from *Bacteroides fragilis*: A Quantum Chemical Study on Model Systems of the Active Site, *J. Am. Chem. Soc.122*, 4197−4208.
33 Diaz, N., Suarez, D., and Merz, K. M. (2001) Molecular Dynamics Simulations of the Mononuclear Zinc-β-lactamase from *Bacillus cereus* Complexed with Benzylpenicillin and a Quantum Chemical Study of the Reaction Mechanism, *J. Am. Chem. Soc.123*, 9867−9879.
34 Prosperi-Meys, C., Wouters, J., Galleni, M., and Lamotte-Brasseur, J. (2001) Substrate Binding, and Catalytic Mechanism of Class B β-Lactamases: A Molecular Modelling Study, *Cell. Mol. Life Sci.58*, 2136−2143.
35 Salsbury, F. R., Crowley, M. F., and Brooks, C. L. (2001) Modeling of the Metallo-β-lactamase from *B. fragilis*: Structural and Dynamic Effects of Inhibitor Binding, *Proteins: Struct., Funct., Genet.44*, 448−459.

36 Suarez, D., and Merz, K. M. (2001) Molecular Dynamics Simulations of the Mononuclear Zinc-β-lactamase from *Bacillus cereus*, *J. Am. Chem. Soc.123*, 3759−3770.
37 Suarez, D., Brothers, E. N., and Merz, K. M. (2002) Insights into the Structure and Dynamics of the Dinuclear Zinc β-Lactamase Site from *Bacteroides fragilis*, *Biochemistry41*, 6615−6630.
38 Suarez, D., Diaz, N., and Merz, K. M. (2002) Molecular Dynamics Simulations of the Dinuclear Zinc-β-lactamase from *Bacteroides fragilis* Complexed with Imipenem, *J. Comput. Chem.23*, 1587−1600.
39 Breece, R. M., Costello, A., Bennett, B., Sigdel, T. K., Matthews, M. L., Tierney, D. L., and Crowder, M. W. (2005) A Five-Coordinate Metal Center in Co(II)-Substituted VanX, *J. Biol. Chem.280*, 11074−11081.
40 Thomas, P. W., Stone, E. M., Costello, A., Tierney, D. L., and Fast, W. (2005) The Quorum-Quenching Lactonase from *Bacillus thuringiensis* Is a Metalloprotein, *Biochemistry44*, 7559−7569.
41 Yang, Y., Keeney, D., Tang, X. J., Canfield, N., and Rasmussen, B. A. (1999) Kinetic Properties and Metal Content of the Metallo-β-lactamase CcrA Harboring Selective Amino Acid Substitutions, *J. Biol. Chem*. *274*, 15706−15711.
42 Toney, J. H., Wu, J. K., Overbye, K. M., Thompson, C. M., and Pompliano, D. L. (1997) High-Yield Expression, Purification, and Characterization of Active, Soluble *Bacteroides fragilis* Metallo-β-lactamase, CcrA, *Protein Expression Purif.9*, 355−362.
43 Paul-Soto, R., Hernandez-Valladares, M., Galleni, M., Bauer, R., Zeppezauer, M., Frere, J. M., and Adolph, H. W. (1998) Mono- and Binuclear Zn-β-lactamase from *Bacteroides fragilis*: Catalytic and Structural Roles of the Zinc Ions, *FEBS Lett.438*, 137−140.
44 Fast, W., Wang, Z., and Benkovic, S. J. (2001) Familial Mutations and Zinc Stoichiometry Determine the Rate-Limiting Step of Nitrocefin Hydrolysis by Metallo-β-lactamase from *Bacteroides fragilis*, *Biochemistry40*, 1640−1650.
45 Paul-Soto, R., Zeppezauer, M., Adolph, H. W., Galleni, M., Frere, J. M., Carfi, A., Dideberg, O., Wouters, J., Hemmingsen, L., and Bauer, R. (1999) Preference of Cd(II) and Zn(II) for the Two Metal Sites in *Bacillus cereus* β-Lactamase II: A Perturbed Angular Correlation of γ-Rays Spectroscopic Study, *Biochemistry38*, 16500−16506.
46 Rasia, R. M., and Vila, A. J. (2002) Exploring the Role and the Binding Affinity of a Second Zinc Equivalent in *B. cereus* Metallo-β-lactamase, *Biochemistry41*, 1853−1860.
47 Dal Peraro, M., Vila, A. J., and Carloni, P. (2002) Structural Determinants and Hydrogen Bond Network of the Mononuclear Zinc(II)-β-lactamase Active Site, *J. Biol. Inorg. Chem.7*, 704−712.
48 Paul-Soto, R., Bauer, R., Frère, J. M., Galleni, M., Meyer-Klaucke, W., Nolting, H., Rossolini, G. M., de Seny, D., Hernandez-Valladares, M., Zeppezauer, M., and Adolph, H. W. (1999) Mono- and Binuclear Zn^{2+}-β-lactamase. Role of the Conserved Cysteine in the Catalytic Mechanism, *J. Biol. Chem.274*, 13242−13249.
49 de Seny, D., Heinz, U., Wommer, S., Kiefer, M., Meyer-Klaucke, W., Galleni, M., Frere, J. M., Bauer, R., and Adolph, H. W. (2001) Metal Ion Binding and Coordination Geometry for Wild Type and Mutants of Metallo-β-lactamase from *Bacillus cereus* 569/H/9 (BcII)A Combined Thermodynamic, Kinetic, and Spectroscopic Approach, *J. Biol. Chem.276*, 45065−45078.
50 Wommer, S., Rival, S., Heinz, U., Galleni, M., Frere, J. M., Franceschini, N., Amicosante, G., Rasmussen, B., Bauer, R., and Adolph, H. W. (2002) Substrate-Activated Zinc Binding of Metallo-β-lactamasesPhysiological Importance of the Mononuclear Enzymes, *J. Biol. Chem.277*, 24142−24147.
51 Periyannan, G., Shaw, P. J., Sigdel, T., and Crowder, M. W. (2004) In Vivo Folding of Recombinant Metallo-β-lactamase L1 Requires the Presence of Zn(II), *Protein Sci.13*, 2236−2243.
52 Bertini, I., and Luchinat, C. (1984) High-Spin Cobalt(II) as a Probe for the Investigation of Metalloproteins, *Adv. Inorg. Biochem.6*, 72−111.
53 Moura, I., Teixeira, M., Legall, J., and Moura, J. J. G. (1991) Spectroscopic Studies of Cobalt and Nickel Substituted Rubredoxin and Desulforedoxin, *J. Inorg. Biochem.44*, 127−139.
54 Davies, A. M., Rasia, R. M., Vila, A. J., Sutton, B. J., and Fabiane, S. M. (2005) Effect of pH on the Active Site of an Arg121Cys Mutant of the Metallo-β-lactamase from *Bacillus cereus*: Implications for the Enzyme Mechanism, *Biochemistry44*, 4841−4849.

1 Abbreviations: ε, extinction coefficient; EDTA, ethylenediaminetetraacetic acid; EPR, electron paramagnetic resonance; EXAFS, extended X-ray absorption fine structure; FPLC, fast protein liquid chromatography; Hepes, 4-(2-hydroxyethyl)-1-piperazineethanesulfonic acid; ICP-AES, inductively coupled plasma spectrometer with atomic emission spectroscopy detection; IPTG, isopropyl β-d-thiogalactoside; MβL's, metallo-β-lactamases; NMR, nuclear magnetic resonance.